Hindawi
Journal of Electrical and Computer Engineering
Volume 2018, Article ID 2972379, 13 pages
https://doi.org/10.1155/2018/2972379

Research Article

A Double Update PWM Method to Improve Robustness for the Deadbeat Current Controller in Three-Phase Grid-Connected System

Ling Yang,[1] **Yandong Chen**,[1] **An Luo**,[1] **Kunshan Huai**,[2] **Leming Zhou**,[1] **Xiaoping Zhou**,[1] **Wenhua Wu**,[1] **Wenjuan Tan**,[1] **and Zhiwei Xie**[1]

[1]*National Electric Power Conversion and Control Engineering Technology Research Center, Hunan University, Changsha 410082, China*
[2]*Guangzhou Power Supply Bureau, Guangzhou 510620, China*

Correspondence should be addressed to Yandong Chen; yandong_chen@hnu.edu.cn

Received 4 March 2018; Accepted 14 May 2018; Published 7 June 2018

Academic Editor: Luigi Piegari

Copyright © 2018 Ling Yang et al. This is an open access article distributed under the Creative Commons Attribution License, which permits unrestricted use, distribution, and reproduction in any medium, provided the original work is properly cited.

In the grid-connected inverter based on the deadbeat current control, the filter inductance variation and single update PWM affect the distortion of the grid current, stability, and dynamic of the system. For this, a double update PWM method for the deadbeat current controller in three-phase grid-connected system is proposed, which not only effectively decreases the grid current distortion and control delay, but also improves the system stability and dynamic response speed due to reducing the characteristic root equation order of the closed-loop transfer function. The influence of the filter inductance deviation coefficient on the system performance is analyzed. As a conclusion, the corresponding filter inductance deviation coefficient in the system critical stability increases with increase in the parasitic resistance of the filter inductance and line equivalent resistance and decreases with increase in the sampling frequency. Considering the system stability and dynamic response, the optimal range of the control parameters is acquired. Simulation and experimental results verify the effectiveness of the proposed method.

1. Introduction

With the increasingly serious energy crisis and environmental pollution, renewable energy distributed generation technology has been widely concerned and researched in [1–4]. The grid-connected inverter is the core of the distributed generation system in [5–8]. Its role is to convert the DC power generated by renewable energy to the AC power accepted by the grid. The deadbeat current control is based on the mathematical model of the grid-connected inverter and depends on the actual electrical parameters of the main circuit. Theoretically, no static-state error can be achieved in [9–12]. Because of its fast current transient response, accurate current tracking characteristic, and all digital control, the deadbeat current control has been applied more often.

However, reliance on the accurate electrical model and control delay are the main constraints in the deadbeat control. On the one hand, the filter inductance value cannot be accurately detected. Even with the increasing of the grid current, the magnetic flux of the filter inductance tends to be saturated, resulting in the decrease of the filter inductance. This will lead to a certain deviation between the model filter inductance and actual filter inductance, affect the control accuracy of the deadbeat control, and cause the grid current distortion in [13, 14]. On the other hand, the inherent delay of the sampling and calculation limits the maximum duty cycle of the grid-connected inverter. For this, the delay caused by the proposed single update PWM in [15] may increase poles of the open-loop pulse transfer function, which affects the stability and dynamic response speed of the system. Therefore, how to improve the stability and dynamic response speed of the system and decrease the distortion of the grid current has become the research focus and goal of the grid-connected inverter.

In [16], a current prediction control method for the inductance online identification is proposed, which can accurately identify the inductance value in static and dynamic processes. An online estimation method of the filter inductance parameter is proposed in [17], which can prevent the current phase difference and system instability when the filter inductance parameter is not matched by the traditional prediction deadbeat current control method. However, the delay caused by the single update PWM has not been considered in the above methods.

The predictive current control technology is proposed to compensate the delay in [15, 18–20]. A supply current predictive controller that adopts the variable step-size adaptive algorithm is proposed in [15], which solves the problem that the maximum duty is limited by the delay caused by the sampling and calculation. Because the weighted coefficient is regulated by the error calculated in each sampling period, this algorithm shows well predictive accuracy. But a single voltage vector is only used in a control cycle, so it needs very high sampling frequency to get good performance [18]. In [19, 20], the linear prediction method is proposed, which can estimate the information of the next beat based on the control object model and the information of the current and past period. Although it eliminates the control delay, this method depends on the accuracy of the model, which may exist a certain estimation error.

At the same time, the current observer is used to predict the next beat current in [10, 21, 22], and the current reference is predicted in advance to compensate for the delay. In [10, 21], the current predictive algorithm based on repetitive control observer is proposed, which solves the problem of the current instability caused by the control delay and improves the current predictive precision. However, this method does not involve the dynamic analysis. In [22], an improved deadbeat current control scheme with a novel adaptive self-tuning load model is proposed. An improved deadbeat current controller with delay compensation is used to achieve high bandwidth current control characteristic, which compensates for the delay of the total system. However, a single prediction algorithm is adopted in the current reference variation, which may cause a large current overshoot or phase lag and deteriorate the system performance.

Digital PWM in double update mode is used to reduce the modulation delays and achieve performance. In [23], the effects of the measurement sampling and PWM updating methods on PI-based current control performance have been studied for a converter system. Reference [24] proposed proportional resonant controller implementation with double update mode digital PWM for single-phase grid-connected inverter. Digitally controlled grid-connected inverters with converter current control scheme and converter current plus grid current control scheme have been studied in [25]. A combination of two samples' time displacement and the line current PWM ripple was proposed to cancel that error and boost the performance of such drives in [26]. Reference [27] demonstrated the improved performance of a three-phase voltage source inverter when digital multi-sampled space vector modulation was used. The bandwidth expansion strategy was proposed to achieve the stator current double sampling and PWM duty cycle double update in a carrier period in [28]. However, the deadbeat current control has not been considered in the above methods. A fast robust PWM method for photovoltaic grid-connected inverter is proposed in [29], which effectively solves the delay of the one-step-delay control and improves the system stability.

In this paper, the double update PWM method to improve robustness for the deadbeat current controller in three-phase grid-connected system is proposed. The paper is organized as follows. Section 2 presents the structure and control method for three-phase grid-connected system. The double update PWM method for the deadbeat current controller is proposed in Section 3. Finally, simulations and experiments are illustrated and discussed in Sections 4 and 5. Some conclusions are given in Section 6.

2. Control Method for Three-Phase Grid-Connected System

Structure of photovoltaic grid-connected system is shown in Figure 1, including the photovoltaic array, inverter circuit, and LC filter. C_{dc} is the DC side storage capacitance, which is used to stabilize the DC voltage U_{dc}. The power transistors Q_1-Q_6 constitute a three-phase full bridge inverter circuit that converts the DC voltage U_{dc} into the AC output voltage, which is the same as the amplitude and phase of the grid voltage. LC filter is formed by the inductance L and capacitance C. In the grid-connected mode, LC filter is equivalent to a single filter inductance. The resistance r is the sum of the parasitic resistance of the filter inductance L and line equivalent resistance. I_{dc} is the DC current. $i_{inv\,j}$ (j=a,b,c) is the inverter output current. $i_{g\,j}$ is the grid current. Since the current flowing through the filter capacitance C is small, $i_{inv\,j}$ is approximately equal to $i_{g\,j}$.

Diagram of the double update PWM method for the deadbeat current controller is shown in Figure 2, including the double closed-loop control and double update PWM. The outer voltage loop adopts the PI control to stabilize U_{dc}. The inner current loop adopts the deadbeat control, which decreases the distortion of the grid current caused by the filter inductance variation. The double update PWM effectively solves the delay caused by the single update PWM and improves the stability and dynamic response speed of the system. U_{dcr} is the DC voltage command, $u_{g\,j}$ is the grid voltage, ω_1 is the fundamental angular frequency of the grid, I_{gr} is the input amplitude command of the inner current loop, $i_{g\,jr}$ is the grid current command, and D_j is the equivalent duty cycle.

3. The Double Update PWM Method for the Deadbeat Current Controller

3.1. The Single Update PWM Method. In digital control, the single update PWM is shown in Figure 3, where u_{ms} is the single update PWM wave. The sampling is carried out at the peak of the (k-1)th triangular carrier. The calculation is based on the sampling value. At the peak of the kth triangular carrier, the single update PWM wave $u_{ms}(k\text{-}1)$ of the (k-1)th

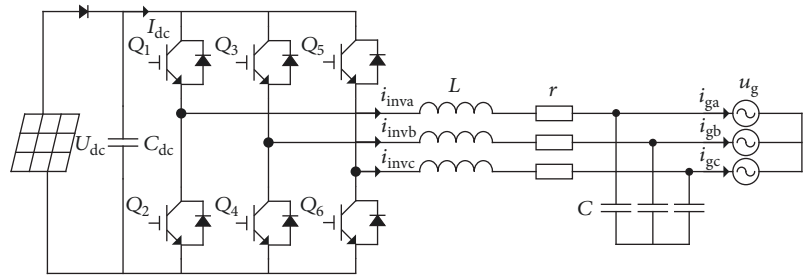

Figure 1: Structure of photovoltaic grid-connected system.

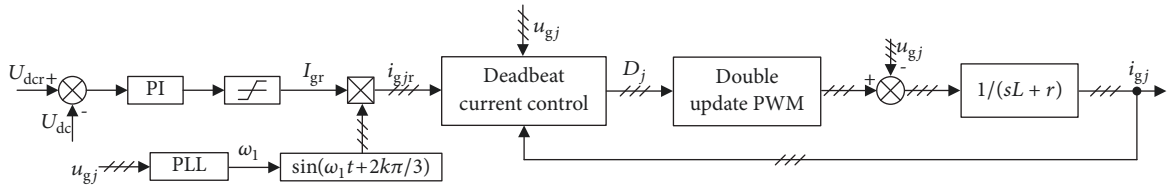

Figure 2: Diagram of the double update PWM method for photovoltaic grid-connected inverter based on the deadbeat control.

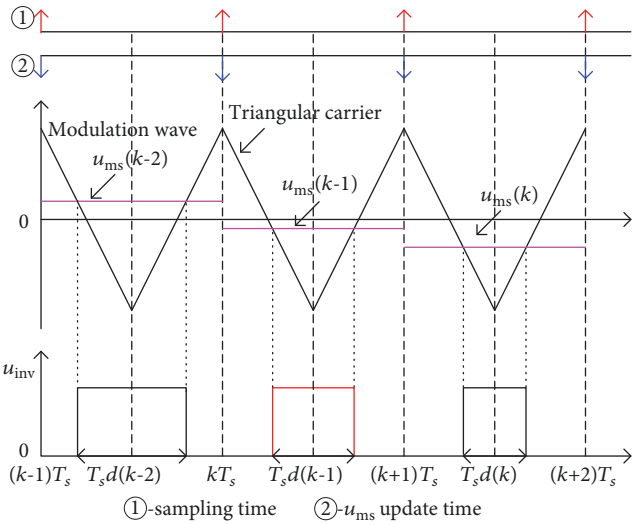

Figure 3: The single update PWM.

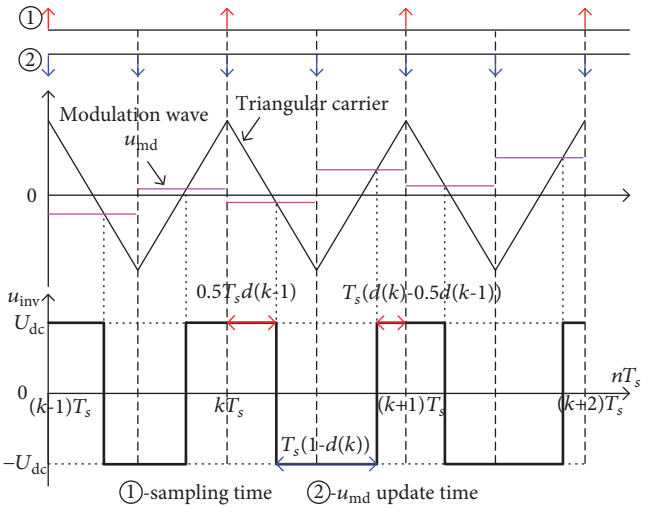

Figure 4: The double update PWM method.

carrier cycle is loaded. So the equivalent duty cycle $D(k)$ of the kth carrier cycle can be expressed as

$$D(k) = d(k-1) \tag{1}$$

where $d(k\text{-}1)$ is the duty cycle calculated by the sampling values at the peak of the $(k\text{-}1)$th triangular carrier.

Obviously, the loading time of the single update PWM wave is lagged behind a sampling period at the beginning of the sampling. So the one-step delay is caused by the single update PWM.

3.2. The Double Update PWM Method. The double update PWM method is shown in Figure 4, where u_{md} is the double update PWM wave. The sampling is carried out at the peak of the triangular carrier. The loading is carried out at the peak and valley of the triangular carrier. That is to say, one sampling and double loading are taken in each carrier cycle. The modulation process is as follows: the sampling is carried out at the peak of the kth triangular carrier. Meanwhile, the double update PWM wave corresponding to the $d(k\text{-}1)$ is loaded, so that the conduction time of the first half of the carrier cycle is $0.5T_sd(k\text{-}1)$. At the valley of the kth triangular carrier, the double update PWM wave corresponding to the difference calculated by subtracting the $d(k\text{-}1)$ from the $2d(k)$ is loaded, so that the conduction time of the second half of the carrier cycle is $T_s(d(k)\text{-}0.5d(k\text{-}1))$. So the equivalent duty cycle $D(k)$ of the kth carrier cycle can be expressed as

$$\begin{aligned} D(k) &= \frac{0.5T_s d(k-1) + T_s(d(k) - 0.5d(k-1))}{T_s} \\ &= d(k) \end{aligned} \tag{2}$$

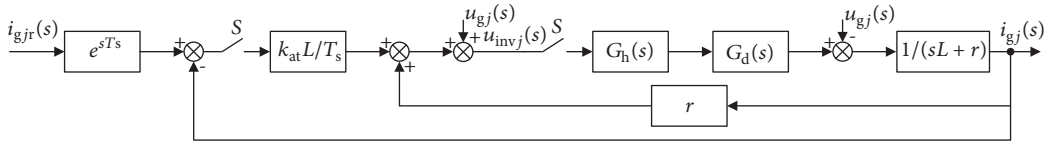

Figure 5: Diagram of the deadbeat current control for the grid-connected inverter.

Table 1: The delay comparison between the single update PWM and proposed method.

Serial number	$G_d(s)$	Method
Case 1	e^{-sTs}	Single update PWM
Case 2	1	Proposed(double update PWM)

where $d(k)$ is the duty cycle calculated by the sampling values at the peak of the kth triangular carrier.

Therefore, the proposed double update PWM method eliminates the control delay. Meanwhile, the time margin of the sampling and calculation decreases from T_s to $T_s/2$.

Diagram of the deadbeat current control for the grid-connected inverter is shown in Figure 5, where $i_{gjr}(s)$ is the input quantity, $u_{gj}(s)$ is the disturbance input quantity, $i_{gj}(s)$ is the output quantity, T_s is the sampling cycle, and S is the synchronous sampling switch. With the increasing of the grid current, the magnetic flux of the filter inductance tends to be saturated, resulting in the decrease of the filter inductance. There is the deviation between the filter inductance L_1 and actual filter inductance L. k_{at} is the filter inductance deviation coefficient. $k_{at}=L_1/L$. $G_h(s)$ is the continuous domain transfer function of the zero order holder (ZOH).

$$G_h(s) = \frac{\left(1 - e^{-sT_s}\right)}{s} \tag{3}$$

$G_d(s)$ is the continuous domain transfer function of the single update PWM, which can be expressed as

$$G_d(s) = e^{-sT_s} \tag{4}$$

The delay comparison between the single update PWM and proposed method is shown in Table 1. Considering the parasitic resistance of the filter inductance and line equivalent resistance, the influence of the control delay on the stability and dynamic of the system is analyzed, and the appropriate control parameter range is given.

3.3. Control System Stability Analysis. In Figure 5, using the single update PWM, $G_d(s)=e^{-sTs}$. $i^*_{gj}(s)$ is Laplace transform of $i_{gj}(s)$, which can be expressed as

$$i^*_{gj}(s) = \frac{k_{at}\left(L/T_s\right)\cdot G_h G_d G^*_L(s)}{1 + \left(k_{at}L/T_s - r\right)\cdot G_h G_d G^*_L(s)} \cdot e^{sT_s} \cdot i^*_{gjr}(s) \tag{5}$$

where $G_L(s)$ is the transfer function of the filter, $G_L(s)=sL+r$, $G_h G_d G_L{}^*(s)$ is Laplace transform of $G_h(s)G_d(s)G_L(s)$, and $i^*{}_{gjr}(s)$ is Laplace transform of the input quantity $i_{gjr}(s)$. By substituting $z=e^{-sTs}$ into (5), the closed-loop pulse transfer function in the z domain is obtained using the single update PWM.

$$\Phi(z) = \frac{k_{at}\left(L/T_s\right)\left(1 - e^{-T_s r/L}\right)\cdot z}{r\left(z - e^{-T_s r/L}\right)z + \left(k_{at}L/T_s - r\right)\left(1 - e^{-T_s r/L}\right)} \tag{6}$$

By substituting $z=(\omega+1)/(\omega-1)$ into (6), the characteristic root equation of the closed-loop transfer function of the system can be obtained as

$$\begin{aligned} &A\omega^2 + B\omega + C = 0 \\ &A = k_{at}\left(\frac{L}{T_s}\right)\left(1 - e^{-T_s r/L}\right) \\ &B = 2r - 2\left(k_{at}\frac{L}{T_s} - r\right)\left(1 - e^{-T_s r/L}\right) \\ &C = r\left(1 + e^{-T_s r/L}\right) \\ &\quad + \left(k_{at}\frac{L}{T_s} - r\right)\left(1 - e^{-T_s r/L}\right) \end{aligned} \tag{7}$$

where ω is transform operator from the z domain to the ω domain.

Based on the Routh criterion [30], the range of the filter inductance deviation coefficient k_{at} can be expressed as

$$0 < k_{at} < \frac{r\left(2 - e^{-T_s r/L}\right)}{1 - e^{-T_s r/L}}\frac{T_s}{L} \tag{8}$$

In Figure 5, using the proposed method, $G_d(s)=1$. The closed-loop pulse transfer function in the z domain can be expressed as

$$\Phi(z) = \frac{k_{at}\left(L/T_s\right)\left(1 - e^{-T_s r/L}\right)\cdot z}{r\left(z - e^{-T_s r/L}\right) + \left(k_{at}L/T_s - r\right)\left(1 - e^{-T_s r/L}\right)} \tag{9}$$

In (6) and (9), compared to the single update PWM, the characteristic root equation order of the closed-loop transfer function of the system is reduced when the proposed method is used.

When $|z| < 1$, the system is stable and the range of the filter inductance deviation coefficient k_{at} can be expressed as

$$0 < k_{at} < \frac{2r}{1 - e^{-T_s r/L}}\frac{T_s}{L} \tag{10}$$

The corresponding filter inductance deviation coefficient in the system critical stability $k_{at\_critical}$ can be expressed as

$$k_{at\_critical} = \frac{2r}{1 - e^{-T_s r/L}}\frac{T_s}{L} \tag{11}$$

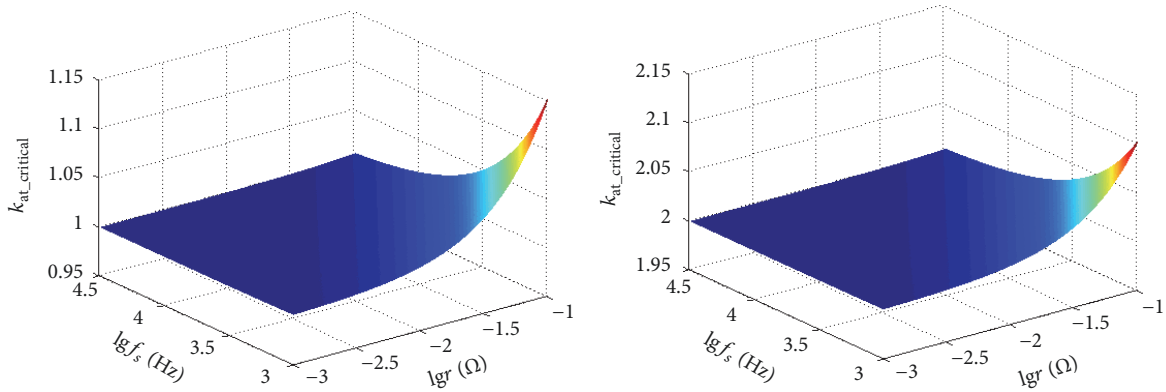

(a) Single update PWM (b) Double update PWM

FIGURE 6: Relationship among the resistance r, sampling frequency f_s, and $k_{at\_critical}$.

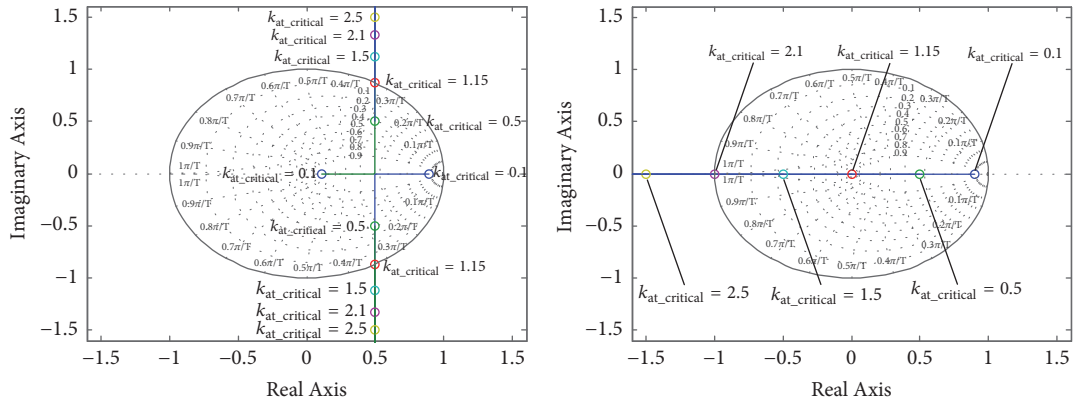

(a) Single update PWM (b) Double update PWM

FIGURE 7: The contrast analysis of root locus with different $k_{at\_critical}$.

Relationship among the resistance r, sampling frequency f_s, and $k_{at\_critical}$ by the single update PWM and proposed method is shown in Figure 6. Figures 6(a) and 6(b) correspond to the single update PWM and proposed method, respectively. When f_s is constant, $k_{at\_critical}$ increases with increase in r. When r is constant, $k_{at\_critical}$ decreases with increase in f_s. When the proposed method is used, the range of $k_{at\_critical}$ is $0< k_{at\_critical} \leq 2.1$, while the range of $k_{at\_critical}$ is $0< k_{at\_critical} \leq 1.15$ by using the single update PWM. So the range of $k_{at\_critical}$ by using the proposed method is obviously larger than the range of $k_{at\_critical}$ by using the single update PWM.

When $k_{at\_critical}$=0.1, 0.5, 1.15, 1.5, 2.1, and 2.5, the root locus analysis with the single update PWM and proposed method is shown in Figure 7. Figures 7(a) and 7(b) correspond to the single update PWM and proposed method, respectively. In Figure 7(a), when $k_{at\_critical}$=0.1 and 0.5, the pole is inside the unit circle, and the system is in a stable state. When $k_{at\_critical}$=1.15, the pole is on the unit circle, and the system is in a critical stable state. When $k_{at\_critical}$=2.1 and 2.5, the pole is outside the unit circle, and the system is in an unstable state.

In Figure 7(b), when $k_{at\_critical}$=0.1, 0.5, 1.15, and 1.5, the pole is inside the unit circle, and the system is in a stable state. When $k_{at\_critical}$=2.1, the pole is on the unit circle, and the system is in a critical stable state. When $k_{at\_critical}$=2.5, the pole is outside the unit circle, and the system is in an unstable state. So the range of $k_{at\_critical}$ by using the proposed method is obviously larger than the range of $k_{at\_critical}$ by using the single update PWM.

3.4. Control System Dynamic Analysis. When the single update PWM is used, system response to unit step change with $k_{at\_critical}$ changing is shown in Figure 8, while the sampling frequency f_s=10kHz and resistance r=0.01Ω are constant. Figures 8(a) and 8(b) correspond to $0< k_{at\_critical} \leq 1$ and $1< k_{at\_critical} \leq 1.15$, respectively. When $0< k_{at\_critical} \leq 1$, the dynamic response of the system is convergent. When $1< k_{at\_critical} \leq 1.15$, the dynamic response of the system is divergent. Therefore, the range of $k_{at\_critical}$ is $0< k_{at\_critical} \leq 1$.

In Figure 8(c), the curves A, B, C, D, E correspond to $k_{at\_critical}$=0.7, 0.5, 0.3, 0.2, 0.1, respectively. In curve C, the system has the best dynamic response and no overshoot when $k_{at\_critical}$ is equal to $k_{at\_critical0}$ ($k_{at\_critical}$=$k_{at\_critical0}$=0.3). In

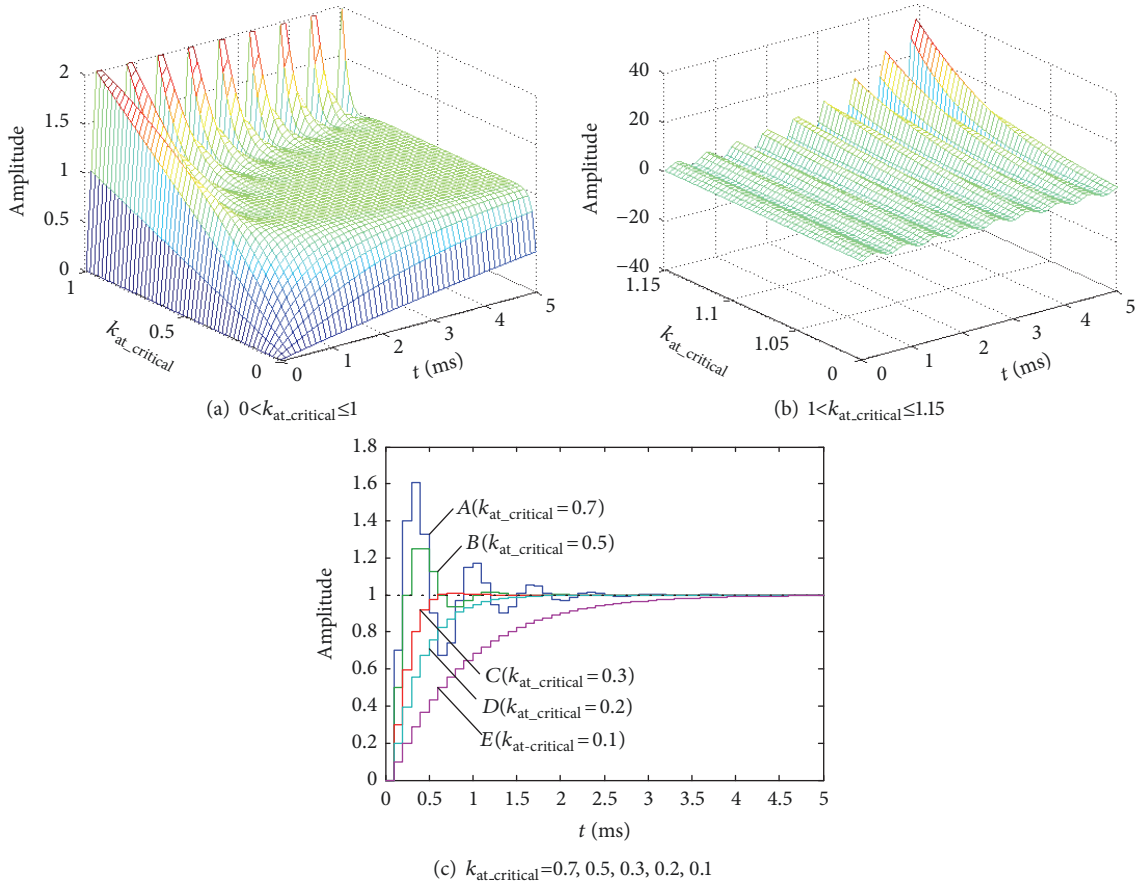

(a) $0<k_{at\_critical}\leq 1$ (b) $1<k_{at\_critical}\leq 1.15$

(c) $k_{at\_critical}$=0.7, 0.5, 0.3, 0.2, 0.1

FIGURE 8: Single update PWM system response to unit step change with the constant sampling frequency f_s=10kHz and resistance r=0.01 when $k_{at\_critical}$ changes.

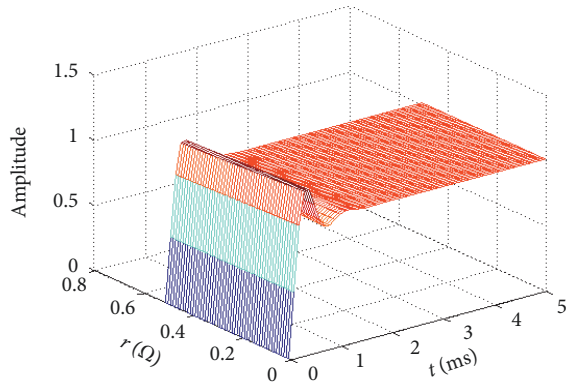

FIGURE 9: Single update PWM system response to unit step change with the constant sampling frequency f_s=10kHz and $k_{at\_critical}$=0.5 when the resistance r changes.

curves A and B, when $k_{at\_critical} > k_{at\_critical0}$, the closed-loop poles are conjugate complex poles located in the right half unit circle of the z plane, and the dynamic response of the system is the oscillation convergence pulse sequence. The smaller $k_{at\_critical}$ is, the closer poles are to the coordinate origin, the smaller the overshoot is, and the faster the response speed is. In curves D and E, when $k_{at\_critical} < k_{at\_critical0}$, the closed-loop poles are located in the real axis of the right half unit circle of the z plane. The dynamic response of the system is unidirectional positive convergence pulse sequence and has no overshoot. The larger $k_{at\_critical}$ is, the closer poles are to the coordinate origin, and the faster the response speed is.

When the single update PWM is used, system response to unit step change with the resistance r changing is shown in Figure 9, while the sampling frequency f_s=10kHz and $k_{at\_critical}$=0.5 are constant. When the resistance r changes, the peak time and the adjustment time of the system do not change much.

When the proposed method is used, system response to unit step change with $k_{at\_critical}$ changing is shown in Figure 10, while the sampling frequency f_s=10kHz and resistance r=0.01Ω are constant. Figures 10(a) and 10(b) correspond to $0< k_{at\_critical} \leq 2$ and $2< k_{at\_critical} \leq 2.1$, respectively. When $0< k_{at\_critical} \leq 2$, the dynamic response of the system is convergent. When $2< k_{at\_critical} \leq 2.1$, the dynamic response of the system is divergent. Therefore, the range of $k_{at\_critical}$ is $0< k_{at\_critical} \leq 2$.

Contrast analysis of system response to unit step change between the single update PWM and proposed method is shown in Figure 11. Curves A and B correspond to

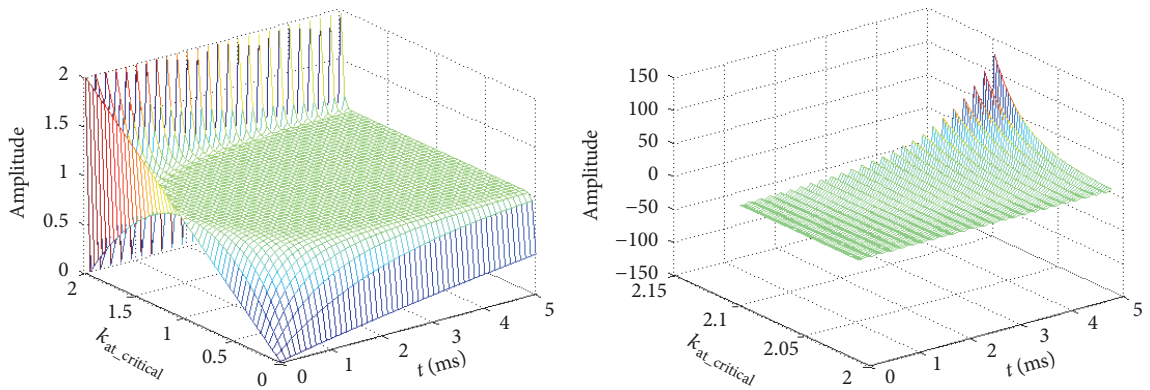

(a) $0<k_{at\_critical}\leq 2$ (b) $2<k_{at\_critical}\leq 2.1$

Figure 10: Proposed control system response to unit step change with the constant sampling frequency f_s=10kHz and resistance r=0.01 when $k_{at\_critical}$ changes.

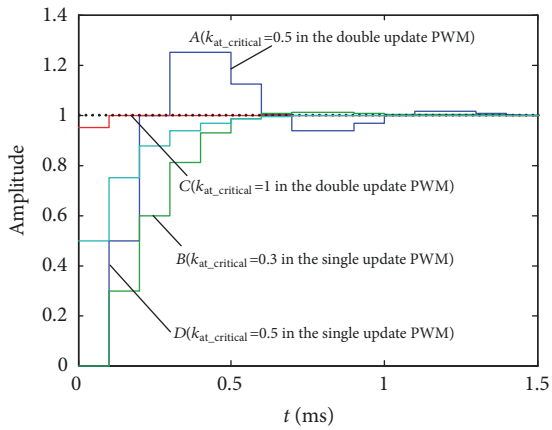

Figure 11: Contrast analysis of system response to unit step change between the single update PWM and proposed method.

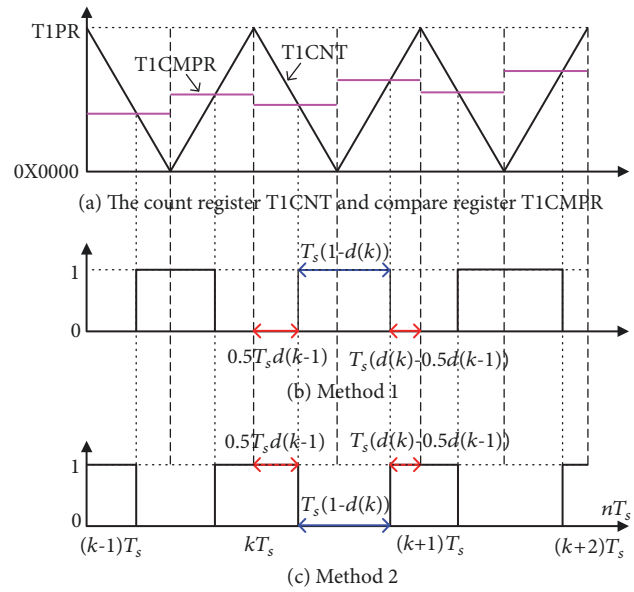

Figure 12: The implementation principle of the proposed modulation method based on the DSP2812 controller.

$k_{at\_critical}$=0.5 and 0.3 in the single update PWM, and curves C and D correspond to $k_{at\_critical}$=1 and 0.5 in the proposed method. Compared to curve D, the system has optimal response to unit step change, fast response speed, and no overshoot in curve C. Comparing curve C with curve B, the optimal response to unit step change of the system in curve C using the proposed method is superior. Comparing curve D with curve A, in curve A using the single update PWM, the unit step response of the system has overshoot, and the oscillation and adjustment time become longer, resulting in the poor dynamic of the system. In curve D using the proposed method, the unit step response of the system has no overshoot and the dynamic becomes better.

3.5. Project Implementation Design Method. The implementation principle of the proposed modulation method based on the DSP2812 controller is shown in Figure 12. DSP adopts TI's TMS320F2812 chip, which is a 32-bit fixed point micro control unit (MCU) with a main frequency of up to 150MHz. And the selected switching frequency is up to 10kHz. The general-purpose timer T1 is set to operate in continuous up/down counting mode. When the value of the count register T1CNT is equal to the period register T1PR, the timer T1 has a cycle interrupt, which starts the AD sampling unit, and (1-$d(k$-1))T1PR is assigned to the compare register T1CMPR. When the value of the count register T1CNT is 0x0000, the timer T1 has an underflow interrupt. The time margin from the start of the sampling to the end of the calculation is $0.5T_s$. The duty cycle $d(k)$ is obtained, and (1-2$d(k)$+$d(k$-1))T1PR is assigned to the compare register T1CMPR. When the value of the count register T1CNT is equal to the compare register T1CMPR, the compare match event occurs, and the level of the pin T1PWM will jump.

Method 1. The compare output pin T1PWM of the timer is set to active high in the DSP2812 controller. The DSP pin output driver signal is shown in Figure 12(b). The drive signal is sent

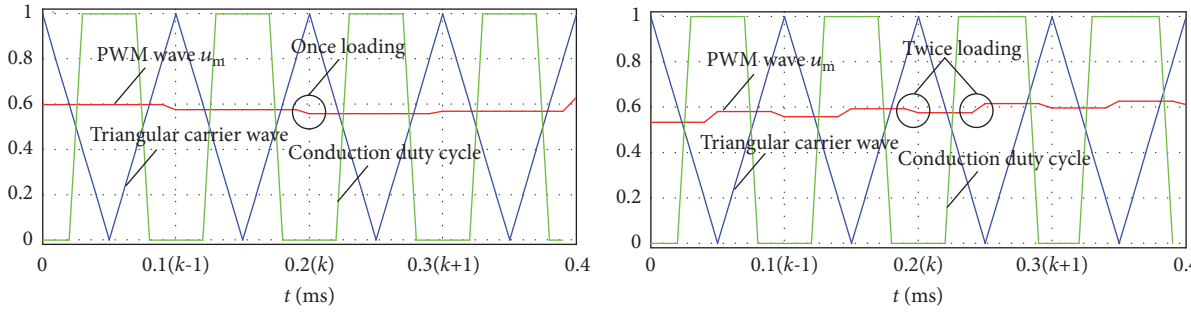

(a) Single update PWM (b) Double update PWM

Figure 13: The simulation waveforms of the modulation wave and triangular carrier wave.

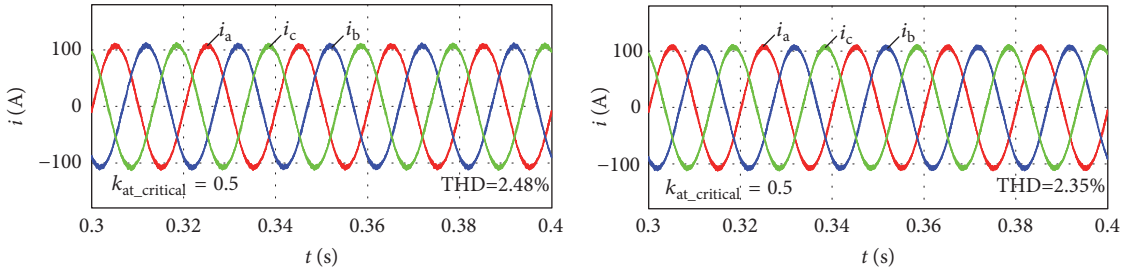

(a) Single update PWM (b) Double update PWM

Figure 14: Steady state simulation waveforms of grid currents with $k_{at\_critical}$=0.5.

to the buffer for isolation and transformation. And then its level is reversed by the phase inverter. The final voltage signal is assigned to the corresponding IPM module.

Method 2. The compare output pin T1PWM of the timer is set to active low in the DSP2812 controller. The DSP pin output driver signal is shown in Figure 12(c). The drive signal is sent to the buffer for isolation and transformation. The final voltage signal is assigned to the corresponding IPM module.

4. Simulation Verification

In order to verify the effectiveness of proposed method, the simulation model of three-phase grid-connected inverter is built by using PSIM 9.0 based on Figure 1. The maximum output power of photovoltaic array is 50kW. System parameters are shown in Table 2.

In order to verify the implementation process of the proposed method, the simulation waveforms of the modulation wave and triangular carrier wave are shown in Figure 13. When the single update PWM and proposed method are used, the modulation processes are similar to the description of Figures 3 and 4. The correctness of the theoretical analysis is verified.

Steady state simulation waveforms of grid currents with $k_{at\_critical}$=0.5 and $k_{at\_critical}$=2 are shown in Figures 14 and 15, respectively. And the steady state simulation results of grid currents are shown in Table 3. In Figure 14(a), when the single update PWM is used with $k_{at\_critical}$=0.5, THD of the grid current is 2.48%. Meanwhile, in Figure 14(b), when the proposed method is used with $k_{at\_critical}$=0.5, THD of the grid current is 2.35%. Under the two modulation methods, the system is in a stable state.

In Figure 15(a), when the single update PWM is used with $k_{at\_critical}$=2, the system is in an unstable state. However, in Figure 15(b), when the proposed method is used with $k_{at\_critical}$=2, THD of the grid current is 2.95%, and the system

Table 2: System parameters.

Parameters and units	Values
DC Voltage U_{dc} [V]	700
DC side storage capacitance C_{dc} [μF]	6000
Filter inductance L [mH]	1.0
Resistance r [Ω]	0.01
Outer voltage loop k_p, k_i	1.5, 0.3
Fundamental frequency f_1 [Hz]	50
Sampling frequency f_s [kHz]	10
Switching frequency f_{sw} [kHz]	10
Carrier frequency f_{tri} [kHz]	10

Table 3: The steady state simulation results of grid currents.

Method	$k_{at\_critical}$	THD
Single update PWM	0.5	2.48%
Proposed method	0.5	2.35%
Single update PWM	2	unstable
Proposed method	2	2.95%

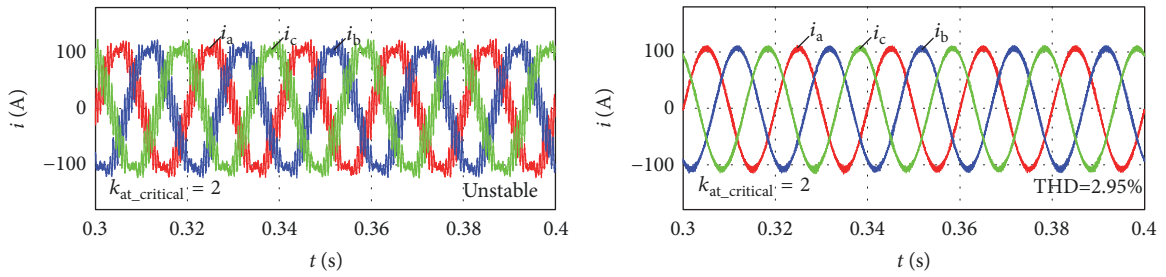

(a) Single update PWM (b) Double update PWM

Figure 15: Steady state simulation waveforms of grid currents with $k_{at\_critical}$=2.

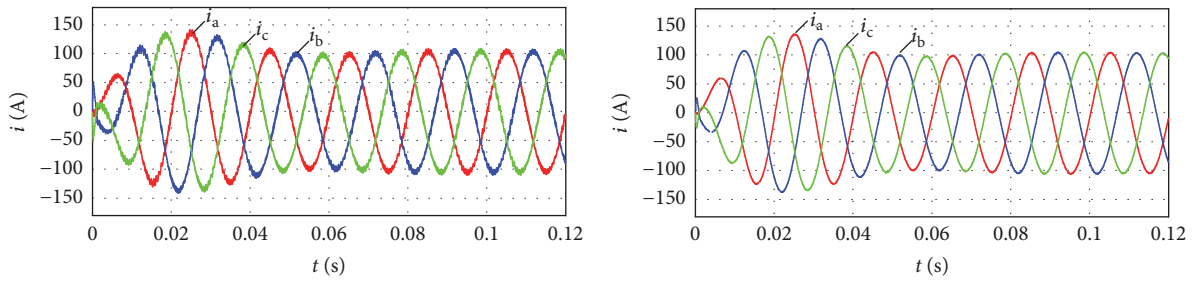

(a) Single update PWM (b) Double update PWM

Figure 16: The dynamic simulation waveforms of grid currents.

Table 4: The dynamic simulation results of grid currents.

Method	Grid inrush current	THD
Single update PWM	50A	2.7%
Proposed method	25A	1.8%

is in a stable state. Therefore, if the value of $k_{at\_critical}$ exceeds its critical range with using the single update PWM, the instability will occur. But when this parameter is applied to the proposed method, the system is still in a stable state. So the range of $k_{at\_critical}$ by using the proposed method is obviously larger than the range of $k_{at\_critical}$ by using the single update PWM.

The dynamic simulation waveforms of grid currents using the single update PWM and proposed method are shown in Figure 16. And the dynamic simulation results of grid currents are shown in Table 4. In Figure 16(a), the grid inrush current is 50A and THD is 2.7% during the start-up process when the single update PWM is used. However, the grid inrush current can be decreased to 25A and THD can be reduced to 1.8% during the start-up process by using the proposed method, as shown in Figure 16(b).

5. Experimentation Verification

In order to verify the validity of simulation results, the experimental platform of three-phase grid-connected system is built shown in Figure 17, which includes the main circuit, the control board, and the LC filter circuit. DSP adopts TI's TMS320F2812 chip, and IGBT selects Infineon

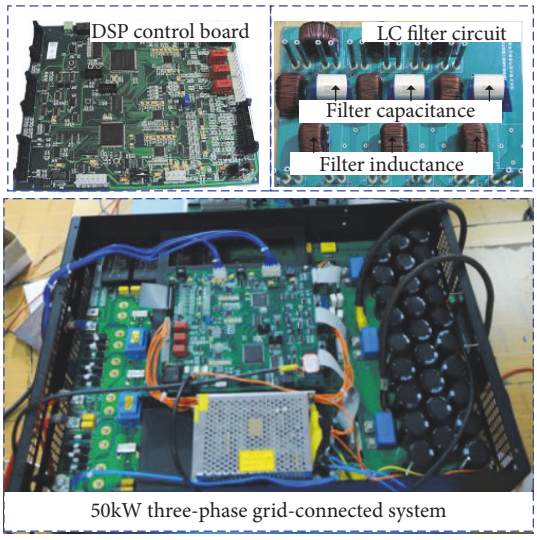

Figure 17: Experimental platform of three-phase grid-connected system.

FF300R12ME4 module. The system parameters are shown as in Table 2.

By real-time debugging and setting breakpoints for the proposed method in CCStudio V3.3, the time spent on the sampling is 11.30μs, the time consumed by the outer voltage loop is 11.80μs, and the time required for the inner current loop is 7.60μs. The total time spent is 30.70μs. The selected switching frequency is up to 10kHz, and the switching period is 100.00μs. Therefore, the time consumed by the sampling

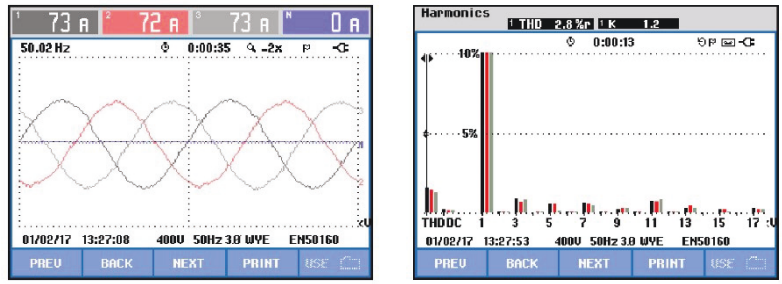

(a) (b)

Figure 18: The experimental waveforms and THD of grid currents using the single update PWM ($k_{at\_critical}$=0.5).

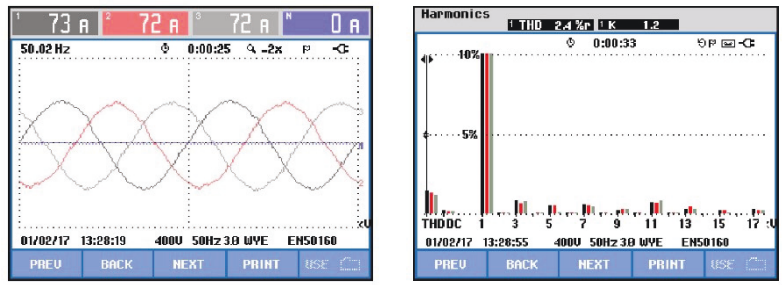

(a) (b)

Figure 19: The experimental waveforms and THD of grid currents using the proposed method ($k_{at\_critical}$=0.5).

Table 5: The steady state experimental results of grid currents.

Method	$k_{at\_critical}$	THD
Single update PWM	0.5	2.8%
Proposed method	0.5	2.4%
Proposed method	1	2.1%
Proposed method	1.5	2.2%

Table 6: The dynamic experimental results of grid currents.

Method	$k_{at\_critical}$	Adjustment time	Overshoot
Single update PWM	0.5	75ms	yes
Single update PWM	0.3	55ms	yes
Proposed method	1	15ms	no
Proposed method	0.5	35ms	no

and calculation is only 30.70% of the switching period, which is less than 0.5 times the switching period. The sampling and calculation can be completed within 0.5 times the switching period.

The steady state experimental results of grid currents are shown in Table 5. And the experimental waveforms and THD of grid currents using the single update PWM and proposed method are shown in Figures 18 and 19, respectively. The theoretical root mean square (RMS) values of the grid currents are 50kW/(3×220V)≈75.76A. Considering some losses, the actual RMS values of grid currents are less than 75.76A. There is a measurement error among three current clamps of FLUKE, so three display values are not equal. Under the same $k_{at\_critical}$=0.5 and control parameters, THD of the grid current using the single update PWM is 2.8%, while THD of the grid current using the proposed method is only 2.4%.

The experimental waveforms and THD of grid currents using the proposed method with $k_{at\_critical}$=1, 1.5 are shown in Figures 20 and 21, respectively. In Figures 19, 20, and 21, THD of the grid current changes from 2.4% to 2.1%, and the next is from 2.1% to 2.2%, showing a tendency to increase firstly and then decrease with the inductance deviation coefficient $k_{at\_critical}$ increasing. Therefore, THD of the grid current is the lowest at $k_{at\_critical}$=1.

Steady state experimental waveforms of grid currents with the single update PWM and proposed method are depicted in Figure 22. In Figure 22(a), when $k_{at\_critical}$ changes from 0.5 to 2 with the single update PWM, the system becomes unstable. However, when $k_{at\_critical}$ changes from 0.5 to 2 with the proposed method, the system can still be in a stable state, as shown in Figure 22(b).

Dynamic experimental waveforms between the single update PWM and proposed method are compared as shown in Figure 23. Figures 23(a) and 23(b) correspond to $k_{at\_critical}$=0.5 and 0.3 in the single update PWM. Figures 23(c) and 23(d) correspond to $k_{at\_critical}$=1 and 0.5 in the proposed method. And the dynamic experimental results of grid currents are as shown in Table 6. The adjustment time is 75ms, 55ms, 15ms, and 35ms, respectively. When the above two individual methods are adopted with $k_{at\_critical}$=0.5, in

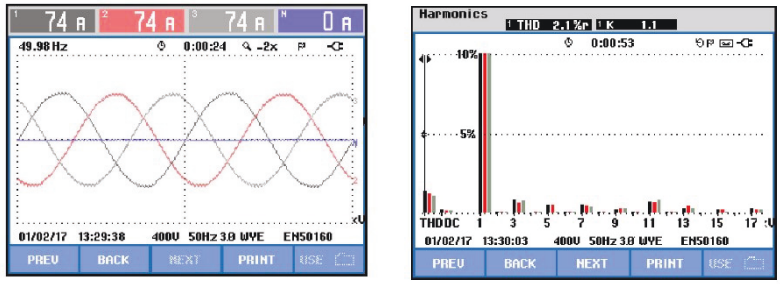

(a) (b)

Figure 20: The experimental waveforms and THD of grid currents using the proposed method ($k_{at\_critical}$=1).

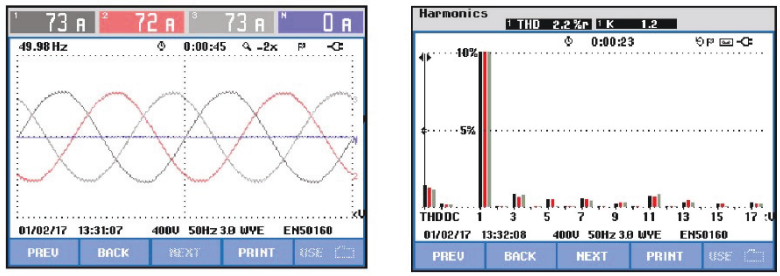

(a) (b)

Figure 21: The experimental waveforms and THD of grid currents using the proposed method ($k_{at\_critical}$=1.5).

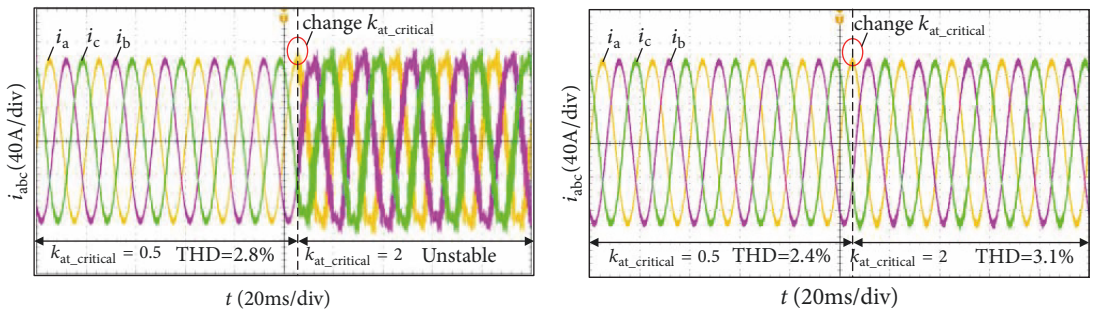

(a) Single update PWM (b) Double update PWM

Figure 22: Steady state experimental waveforms of grid currents with the single update PWM and proposed method.

Figure 23(a), the system has overshoot, and the adjustment time becomes longer, resulting in the poor dynamic. However, in Figure 23(d), the system has no overshoot and the dynamic becomes better with using the proposed method. Comparing Figure 23(c) with Figure 23(d), the adjustment time of the former is only 15ms, while the latter is 35ms. Thus, the system has faster response speed when the proposed method is used with $k_{at\_critical}$=1. Comparing Figure 23(a) with Figure 23(b), the system has the better dynamic with $k_{at\_critical}$=0.3 rather than $k_{at\_critical}$=0.5 when the single update PWM is used. From Figures 23(c) and 23(b), it can be obtained that the optimal dynamic of the system is superior by using the proposed method. The experimental results prove the correctness of theoretical analysis for Figure 11.

6. Conclusion

In this paper, the proposed double update PWM method for the deadbeat current controller not only effectively decreases the grid current distortion and control delay, but also improves the system stability and dynamic response speed due to reducing the characteristic root equation order of the closed-loop transfer function. The influence of the filter inductance deviation coefficient on the system performance is analyzed. As a conclusion, the corresponding filter inductance deviation coefficient in the system critical stability increases with increase in the parasitic resistance of the filter inductance and line equivalent resistance and decreases with increase in the sampling frequency.

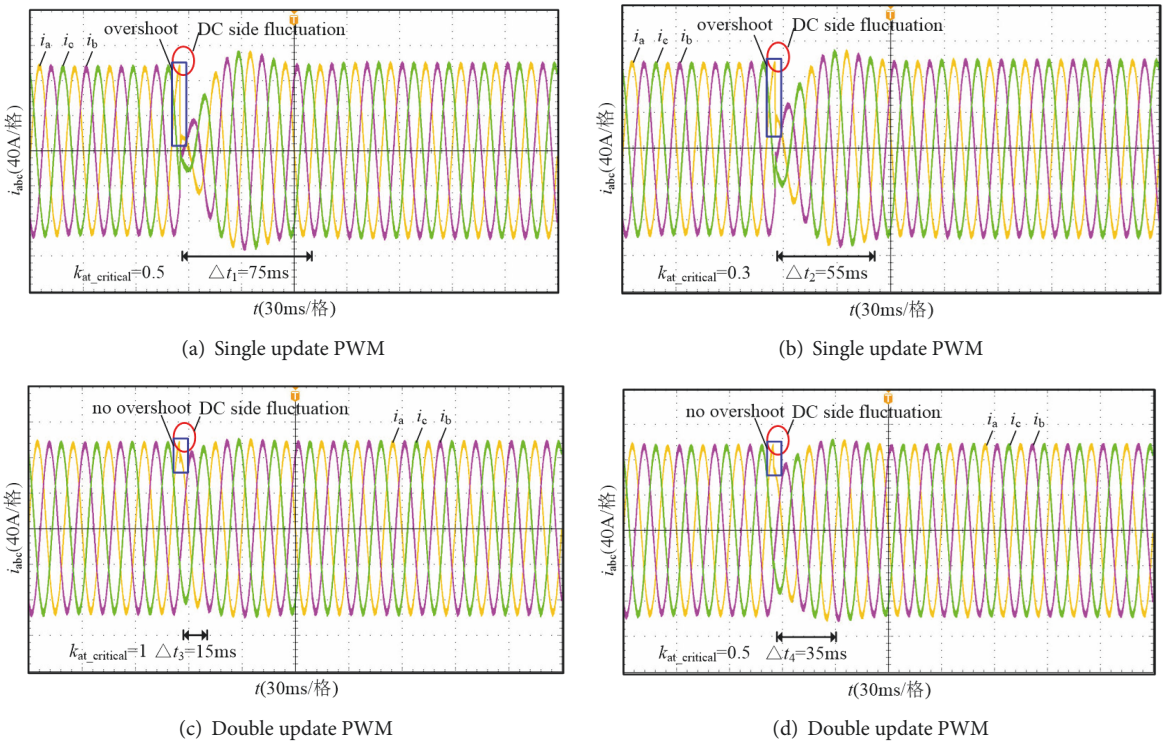

(a) Single update PWM (b) Single update PWM

(c) Double update PWM (d) Double update PWM

Figure 23: Contrast analysis of dynamic experimental waveforms between the single update PWM and proposed method.

Data Availability

Some data are included within the article. No additional data are available.

Conflicts of Interest

The authors declare that they have no conflicts of interest.

Acknowledgments

This work was supported by the National Natural Science Foundation of China under Grant no. 51577056 and no. 51707061 and the Hunan Provincial Innovation Foundation for Postgraduate no. CX2017B104.

References

[1] M. Yazdanian and A. Mehrizi-Sani, "Distributed control techniques in microgrids," *IEEE Transactions on Smart Grid*, vol. 5, no. 6, pp. 2901–2909, 2014.

[2] Y. Li, Y. Zhou, F. Liu, Y. Cao, and C. Rehtanz, "Design and Implementation of Delay-Dependent Wide-Area Damping Control for Stability Enhancement of Power Systems," *IEEE Transactions on Smart Grid*, vol. 8, no. 4, pp. 1831–1842, 2017.

[3] L. Zhou, Y. Chen, A. Luo et al., "Robust two degrees-of-freedom single-current control strategy for LCL-type grid-connected DG system under grid-frequency fluctuation and grid-impedance variation," *IET Power Electronics*, vol. 9, no. 14, pp. 2682–2691, 2016.

[4] Z. Shuai, Y. Hu, Y. Peng, C. Tu, and Z. J. Shen, "Dynamic Stability Analysis of Synchronverter-Dominated Microgrid Based on Bifurcation Theory," *IEEE Transactions on Industrial Electronics*, vol. 64, no. 9, pp. 7467–7477, 2017.

[5] V. V. S. Pradeep Kumar and B. G. Fernandes, "A Fault-Tolerant Single-Phase Grid-Connected Inverter Topology with Enhanced Reliability for Solar PV Applications," *IEEE Journal of Emerging and Selected Topics in Power Electronics*, vol. 5, no. 3, pp. 1254–1262, 2017.

[6] A. Luo, Y. Chen, Z. Shuai, and C. Tu, "An improved reactive current detection and power control method for single-phase photovoltaic grid-connected dg system," *IEEE Transactions on Energy Conversion*, vol. 28, no. 4, pp. 823–831, 2013.

[7] C. Yoon, H. Bai, R. N. Beres, X. Wang, C. L. Bak, and F. Blaabjerg, "Harmonic stability assessment for multiparalleled, grid-connected inverters," *IEEE Transactions on Sustainable Energy*, vol. 7, no. 4, pp. 1388–1397, 2016.

[8] Y. Li, F. Liu, L. Luo, C. Rehtanz, and Y. Cao, "Enhancement of commutation reliability of an HVDC inverter by means of an inductive filtering method," *IEEE Transactions on Power Electronics*, vol. 28, no. 11, pp. 4917–4929, 2013.

[9] X. Zhang, B. Hou, and Y. Mei, "Deadbeat Predictive Current Control of Permanent-Magnet Synchronous Motors with Stator Current and Disturbance Observer," *IEEE Transactions on Power Electronics*, vol. 32, no. 5, pp. 3818–3834, 2017.

[10] W. Jiang, W. Ma, J. Wang, L. Wang, and Y. Gao, "Deadbeat Control Based on Current Predictive Calibration for Grid-Connected Converter under Unbalanced Grid Voltage," *IEEE Transactions on Industrial Electronics*, vol. 64, no. 7, pp. 5479–5491, 2017.

[11] M. Pichan, H. Rastegar, and M. Monfared, "Deadbeat Control of the Stand-Alone Four-Leg Inverter Considering the Effect of the Neutral Line Inductor," *IEEE Transactions on Industrial Electronics*, vol. 64, no. 4, pp. 2592–2601, 2017.

[12] F. Blaabjerg, R. Teodorescu, M. Liserre, and A. V. Timbus, "Overview of control and grid synchronization for distributed power generation systems," *IEEE Transactions on Industrial Electronics*, vol. 53, no. 5, pp. 1398–1409, 2006.

[13] J. C. Moreno, J. M. Espí Huerta, R. G. Gil, and S. A. Gonzalez, "A robust predictive current control for three-phase grid-connected inverters," *IEEE Transactions on Industrial Electronics*, vol. 56, no. 6, pp. 1993–2004, 2009.

[14] J. He, Y. W. Li, D. Xu, X. Liang, B. Liang, and C. Wang, "Deadbeat Weighted average current control with corrective feed-forward compensation for microgrid converters with nonstandard LCL filter," *IEEE Transactions on Power Electronics*, vol. 32, no. 4, pp. 2661–2674, 2017.

[15] B. Liu, Y. Zha, and T. Zhang, "D-Q frame predictive current control methods for inverter stage of solid state transformer," *IET Power Electronics*, vol. 10, no. 6, pp. 687–696, 2017.

[16] S. Liu, K. Wu, and Y. Tzou, "Control of a single-phase grid inverter with on-line inductance identification," in *Proceedings of the 2016 IEEE 25th International Symposium on Industrial Electronics (ISIE)*, pp. 454–459, Santa Clara, CA, USA, June 2016.

[17] C. Chen, L. Li, Q. Zhang et al., "Online inductor parameters identification by small-signal injection for sensorless predictive current controlled boost converter," *IEEE Transactions on Industrial Informatics*, vol. 13, no. 4, pp. 1554–1564, 2017.

[18] Z. Deng and W. Song, "Inductance sensitivity analysis of model predictive direct current control strategies for single-phase PWM converters," in *Proceedings of the 2015 IEEE 2nd International Future Energy Electronics Conference (IFEEC)*, pp. 1–6, Taipei, Taiwan, November 2015.

[19] S. Bibian and H. Jin, "Time delay compensation of digital control for DC switchmode power supplies using prediction techniques," *IEEE Transactions on Power Electronics*, vol. 15, no. 5, pp. 835–842, 2000.

[20] H. Kim, J. Han, Y. Lee, J. Song, and K. Lee, "Torque predictive control of permanent-magnet synchronous motor using duty ratio prediction," in *Proceedings of the 2013 IEEE 22nd International Symposium on Industrial Electronics (ISIE)*, pp. 1–5, Taipei, Taiwan, May 2013.

[21] C. Li, S. Shen, J. Zhang, M. Guan, and J. Lu, "Deadbeat Control Based on New State-observer for PWM Rectifier," in *Proceedings of the 2006 Chinese Control Conference*, pp. 1991–1995, Harbin, China, August 2006.

[22] J. M. Espí, J. Castelló, R. García-Gil, G. Garcerá, and E. Figueres, "An adaptive robust predictive current control for three-phase grid-connected inverters," *IEEE Transactions on Industrial Electronics*, vol. 58, no. 8, pp. 3537–3546, 2011.

[23] N. Hoffmann, F. W. Fuchs, and J. Dannehl, "Models and effects of different updating and sampling concepts to the control of grid-connected PWM convertersa study based on discrete time domain analysis," in *Proceedings of the European Conference on Power Electronics and Application*, p. 10, Appl., Birmingham, United kingdom, August-September, 2011.

[24] J. K. Pandit, B. Sakthisudhursun, and M. V. Aware, "PR controller implementation using double update mode digital PWM for grid connected inverter," in *Proceedings of the 2014 IEEE International Conference on Power Electronics, Drives and Energy Systems (PEDES)*, pp. 1–6, Mumbai, India, December 2014.

[25] X. Zhang, J. W. Spencer, and J. M. Guerrero, "Small-signal modeling of digitally controlled grid-connected inverters with LCL filters," *IEEE Transactions on Industrial Electronics*, vol. 60, no. 9, pp. 3752–3765, 2013.

[26] D. P. Marcetic and E. M. Adžić, "Improved three-phase current reconstruction for induction motor drives with DC-Link shunt," *IEEE Transactions on Industrial Electronics*, vol. 57, no. 7, pp. 2454–2462, 2010.

[27] G. Oriti and A. L. Julian, "Three-phase VSI with FPGA-based multisampled space vector modulation," *IEEE Transactions on Industry Applications*, vol. 47, no. 4, pp. 1813–1820, 2011.

[28] H. Wang, M. Yang, L. Niu et al., "Current-loop bandwidth expansion strategy for permanent magnet synchronous motor drives," in *Proceedings of the 2010 5th IEEE Conference on Industrial Electronics and Applications (ICIEA)*, pp. 1340–1345, Taichung, Taiwan, June 2010.

[29] L. Yang, A. Luo, Y. Chen et al., "A fast robust PWM method for photovoltaic grid-connected inverter," in *Proceedings of the IECON 2017 - 43rd Annual Conference of the IEEE Industrial Electronics Society*, pp. 4811–4816, Beijing, October 2017.

[30] E. J. Mastascusa, W. C. Rave, and B. M. Turner, "Polynomial Factorization using the Routh Criterion," *Proceedings of the IEEE*, vol. 59, no. 9, pp. 1358-1359, 1971.

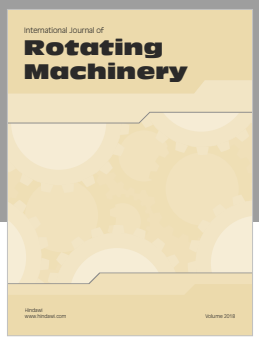

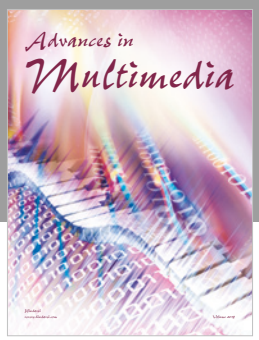

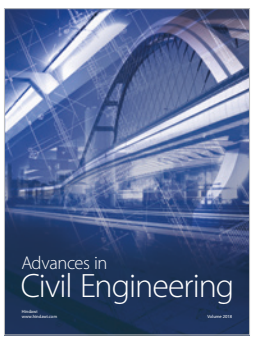

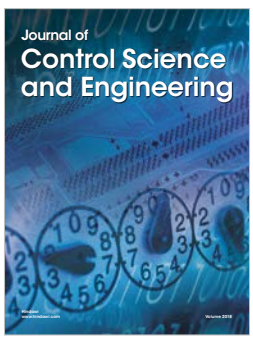

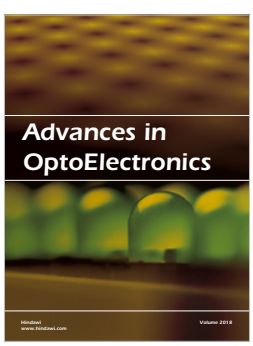

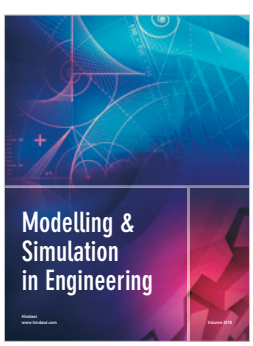

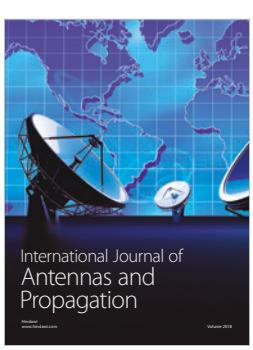

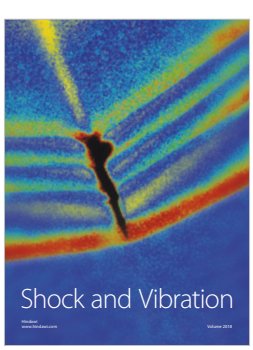

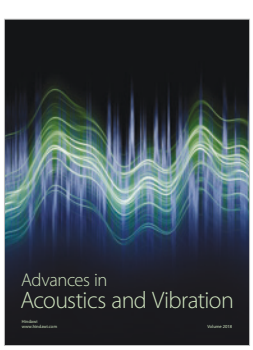

Hindawi

Submit your manuscripts at
www.hindawi.com